Published 1/31; corrected 2/1/2013

www.sciencemag.org/cgi/content/full/339/6119/574/DC1

Supplementary Materials for

Emergent Sensing of Complex Environments by Mobile Animal Groups

Andrew Berdahl,* Colin J. Torney, Christos C. Ioannou, Jolyon J. Faria, Iain D. Couzin*

*To whom correspondence should be addressed. E-mail: aberdahl@princeton.edu (A.B.); icouzin@princeton.edu (I.D.C.)

Published 1 February 2013, *Science* **339**, 574 (2013)
DOI: 10.1126/science.1225883

This PDF file includes

Corrected 2/1/2013 to include full references.

1 Materials and Methods

1.1 Experimental protocol

We obtained 750 juvenile Golden shiners (*Notemigonus crysoleucas*) (4.9 ± 0.5 cm body length at time of testing) from a commercial live bait supplier (Anderson Minnow Farm, Arkansas, U.S.A.). We kept fish under laboratory conditions, $18\,^{\circ}\mathrm{C}$, 1000μS salinity with a 13:11 day:night light cycle, for 2 weeks before the start of, and throughout, the experiment. The fish resided in 27 gallon black plastic stock tanks, with approximately 150 fish per tank, and were fed 4 times daily with a mix of Zeigler High-Protein Finfish Starter Feed (Z) and Golden Pearl reef and larval fish diet (GP) at a ratio of 4:1, Z:GP.

The experimental arena was 213×122 cm, made of white acrylic Plexiglas and filled with aged water to a depth of 8cm. We projected dynamic light gradients, ranging from 4.2-150 lux, from an Epson PowerLite 1730W Multimedia Projector, directly downward from a height of 240cm, directly above the tank, onto the opaque bottom of the tank in an otherwise dark room. Additionally we illuminated the underside of the tank, which was semi-transparent in the infrared (IR) spectrum, uniformly with IR light, using 9 Lorex VQ2121 Infrared Night Vision illuminators. See Figure S1 for a schematic view.

We conducted all experiments between 9am and 1pm. Each morning we transferred the fish to be used that day into a holding tank identical to the tank in which they were housed. There we let them acclimatise for 30 minutes. For each trial we selected the appropriate number of fish at random and transferred them to the experimental arena. Following a 5 minute acclimatization period, in which fish experienced an even, low (4.2 lux) illumination, we presented the fish with 4 six-minute dynamic light gradients all with the same noise level. Between each six-minute trial was a 1 minute interlude period with low (4.2 lux) illumination. After the 4 trials we moved the fish to a separate holding tank so that they would not be used again that day. We then moved

to the next group size, selecting the appropriate number of fish from the holding tank, let them habituate for 5 minutes and repeated the process.

On each day of testing we used 4 unique projections, all with the same level of noise. The four trials conducted with each group of fish on a single day corresponded to these 4 projections. Each group size was tested once per day, with the order of testing being randomized. See Table S1 for the experimental schedule. The sequence of testing within each group had no effect on relative performance ($\chi^2_1 = 0.52$, $P = 0.47$, Linear Mixed Model). Across days, the order in which different noise levels were tested was also randomized. Additionally we randomized the order of the housing tanks from which we took the fish each day, with the constraint that there would be at least two days between the use of a single tank, so that any fish could be used at most once every three days.

Group sizes 1, 128 and 256 were tested, over 8 days, after the other group sizes, according to the same experimental procedure. During this period fish were used at *most* once every two days. Although larger groups were tested toward the end of the experimental program, we found no improvement over the first fifteen days of the experiments (group sizes 2-64 were performed in this period). Thus there is no evidence that fish were 'learning' to solve this task as the experiment progressed.

In total, for each combination of group size and noise, except 256, we performed 20, six minute, replicates. For group size 256, due to limitations on the number of fish available, four replicates at each noise level were performed.

To ensure fish were visible to the camera when moving from light to dark regions, we recorded the trials, from above, and in IR, with a Sony HDR-XR550V HD Handycam Camcorder outfitted with a Tiffen 37mm #87 Infrared Filter (IR pass) filter. From this footage we obtained the positions and speeds of the fish. To synchronize the IR footage with the light projections we also filmed the trials in visible light with a Canon DM-XM2 E equipped with a

Canon WD-58H 58mm 0.7x wide angle converter lens. We controlled the cameras and projector remotely, out of sight of the experimental arena.

All experiments were conducted in accordance with federal and state regulations, and were approved by the Princeton University Institutional Animal Care and Use Committee.

1.2 Metrics

Group performance We calculate the mean gradient tracking performance for a trial, ψ, as follows. First we calculate the mean level of darkness, $(1 - L)$, of a trial over fish and over time,

$$\psi = \Big\langle \langle 1 - L \rangle_{fish} \Big\rangle_t \tag{1}$$

where $<>_{fish}$ and $<>_t$ denote averages over fish locations and time respectively. In a similar fashion, we calculate a null performance, ψ_{null}, by averaging the mean level of darkness along the fish trajectories as if they had been experiencing the temporal average of the light field. To do so we use Equation 1 but replace L by its temporal average, which varies in space but not time. We then divide the raw performance by the null performance to get $\Psi = \psi/\psi_{null}$. This relative measure allows us to control for any spatial use patterns not related to the light field, as explained in Section 1.3.

To obtain the theoretical maximum for the tracking performance we calculated ψ along the path that minimized the null performance, ψ_{null}, while remaining within the dark patch for the entire trial (i.e. $\psi = 1$). We did this for each light field we used and averaged over fields to obtain $\Psi_{max} = 3.2 \pm 0.5$. Note that this assumes perfect tracking of the light field and no restriction on swim speed or turning rates. In reality, even if fish could track the gradient perfectly they would not have access to the information needed to minimize ψ_{null}, thus Ψ_{max} is an upper bound on the set of performances that track the dark patch perfectly.

Social vector The social vector, $\mathbf{S}$, is the sum of the unit vectors pointing from the focal fish to

its conspecifics,

$$\mathbf{S}_i = \sum_{j \in r_s, j \neq i} \frac{\mathbf{c}_j - \mathbf{c}_i}{|\mathbf{c}_j - \mathbf{c}_i|}. \tag{2}$$

where $\mathbf{c}_i$ is the position of the i^{th} fish and the sum is over all neighbors within an assumed range of interaction of the focal fish, r_s, that is if $1 \leq |\mathbf{c}_j - \mathbf{c}_i| \leq r_s$ (we discount neighbors within one body length so as to not consider repulsive interactions that predominate at this scale). The direction of the social vector indicates the direction of social attraction and its length is a proxy for the strength of the attraction. We have used $r_s = 7$ body lengths in Figures 2B and 2C, while in Figure S16 we show results for different values of this range.

Environmental vector We take the environmental vector (due to the light gradient), $\mathbf{G}$, to be the negative gradient of the light field, L, evaluated at the position, $\mathbf{c}_i$, of the focal fish,

$$\mathbf{G}_i = -\nabla L\Big|_{\mathbf{c}_i} = -\hat{\mathbf{x}}\frac{\partial L}{\partial x}\Big|_{\mathbf{c}_i} - \hat{\mathbf{y}}\frac{\partial L}{\partial y}\Big|_{\mathbf{c}_i}. \tag{3}$$

It points in the direction with the greatest increase in darkness, and its length is the rate of change of light in that direction.

To calculate the response of an individual fish to their social and environmental vectors we found the correlation between the direction of those vectors and the direction of acceleration of that fish, as follows,

$$\text{individual response to social vector} = \left\langle \frac{\mathbf{S}_i}{|\mathbf{S}_i|} \cdot \frac{\mathbf{a}_i}{|\mathbf{a}_i|} \right\rangle_t \tag{4}$$

$$\text{individual response to environmental vector} = \left\langle \frac{\mathbf{G}_i}{|\mathbf{G}_i|} \cdot \frac{\mathbf{a}_i}{|\mathbf{a}_i|} \right\rangle_t \tag{5}$$

where $<>_t$ denotes an average over time.

1.3 Controls

Since the temporal mean of our light fields was not spatially invariant (the middle of the tank tended to be slightly darker), if a group of fish had some natural tendency to spend more time

in the center of the tank, regardless of light levels, they would appear to track the gradient more successfully than a would group that preferred the remain near the edges of the tank.

Thus to control for other effects of group size, such as space use within the tank, irrespective of the light field, we calculate a null performance for each trial by scoring the fish as though they were experiencing the temporal average of all light fields used, rather than the light field they were actually experiencing. This accounts for any spatial use patterns not related to the light field. We then divide the original performance by the null performance (control) to obtain the unbiased performance metric that is reported in Figure 1B of the main text.

Similarly the measure of swim speed as a function of light level (Figure 2A & Figure S12) could be sensitive to spatial correlations in light and speed. For example, if the fish tended to swim more quickly in the middle of the tank independently of light level, but on average the middle of the tank were darker, it would appear that the fish swim more quickly in darker areas.

To account for this, in addition to calculating the swim speed of the fish as a function of the local light level they were experiencing, we also computed a control. For the control, the swim speed of each fish as a function of light level was calculated using a light field different from the one they experienced in the actual trial (but with the same noise level). In this case the movements of the fish should be independent of the light field, but that light field had the same statistical properties as the one they did experience. We calculated the mean swim speed as a function of light level for 4 different control light fields, averaged those values and subtracted them from the speed versus light curve obtained from the actual light field they experienced. This is the reason for negative speeds in Figure 2A. A similar analysis was conducted for density shown in Figure S14. We calculated mean nearest neighbor distance as a function of light level for 4 different control light fields, averaged those and subtracted that from the curve of nearest neighbour distance versus light level derived from the light field the fish had actually experienced.

1.4 Statistical methods

Statistical analysis of performance relative to the control ($\Psi = \psi/\psi_{null}$) as a function of group size and noise level, was conducted using Linear Mixed Models in R (version 2.14.1). The interaction between these two explanatory variables was included in the model, as well as a main effect of sequence in group (1st to 4th trial) to test for any habituation/training effect as the trials progressed within a group of fish. Group identity and projection identity were included as crossed random effects. Significance of the interaction was determined first by comparing models with and without this term, then main effects were tested by their removal from the main-effects model of all three terms where the other two main effects remained in the model. The degrees of freedom presented in the statistical results is the difference in the number of parameters between the two models being compared. Model residuals were homoscedastic and approximately normally distributed throughout.

To estimate error bars in Figure 2 of the main text, we down-sample, taking measurements once every three seconds (positive autocorrelation in speed exists for approximately two seconds). For speed-light calculations (Figure 2A), where spatial correlations are present, we select a single individual at random at each time step to remove any potential spatial or inter-individual autocorrelation either in speed or light level.

1.5 Generation of the illumination field

The following details the methodology behind the development of the stochastic illumination field used in the experiments. The field was generated using `C++` and the open source software packages `PNGwriter` and `ffmpeg`.

In summary, the light gradient consists of the supposition of two fields, a moving circular region and a spatio-temporal multi-frequency noise field. The circular field created a larger

scale light profile that moved throughout the tank, and was defined by

$$f(\mathbf{x}) = \max\left(1.0, 1.5\exp\left[-\frac{|\mathbf{x}-\mathbf{c}|}{D}\right]\right) \tag{6}$$

where D is a parameter determining the length scale of the region (see Table S2 for values). The motion of the center of this region, defined by $\mathbf{c}$, was controlled by a process of selecting a random set of coordinates within the projected arena, moving towards those coordinates, and then once at those coordinates, repeating the first step. To add further noise to this gradient, a dynamic noise field was incorporated. The relative weighting of this noise was varied and three different values were used (see Figure S2).

To create the spatio-temporal noise, a process involving the random evolution of the Fourier modes of the field was used (*28*). This process generates a stochastic scalar field with zero mean that has the following properties

- it is statistically stationary, meaning the properties of the field do not change over time
- it is homogeneous i.e. all areas of the domain are equivalent
- and it is isotropic, meaning a rotation of the field has no effect.

We refer to this real-valued, scalar field as $\chi(x,t)$. To ensure the field is homogeneous and stationary χ is taken to be a solution to the stochastic partial differential equation

$$\frac{\partial \chi}{\partial t} = \nu\nabla^2\chi + \sqrt{\xi}\frac{\partial W}{\partial t} \tag{7}$$

W is a coloured noise term, white in time, with a prescribed spectrum that defines the energy spectrum of the field,

$$W(x,t) = \sum_{k\in\mathbf{K}} \sqrt{\lambda_k} e^{ik\cdot x}\hat{W}_k \tag{8}$$

where $\hat{W}_k$ are Brownian motions subject to the constraint $\hat{W}_k = \hat{W}^*_{-k}$, i.e. certain values are complex conjugates of one another to ensure the field remains real-valued. For λ_k we employ a

spectrum with an exponential decay, defined as

$$\lambda_k \propto |k|^2 \exp\left[-\frac{|k|^2}{k_0^2}\right] \tag{9}$$

and subject to the normalizing condition,

$$\sum_{k\in\mathbf{K}} \lambda_k = 1 \tag{10}$$

The characteristic length scale of the noise field is therefore determined by the largest magnitude energy mode, $|k| = k_0$ (see Table S2 for parameter values used in the simulations and the experiments). The parameter ν acts as viscosity that dampens the fluctuations in the field and controls the temporal correlations, while ξ defines the magnitude of the variability in the field. Since we will later scale this noise field in relation to the magnitude of the large scale circular patch, we set $\xi = 1$.

To solve Eqn. 7 we decompose into the individual Fourier modes. As this is a linear equation each mode can be solved independently and this leads directly to a system of Ornstein-Uhlenbeck equations of the form

$$d\hat{\chi}_k = -\nu|k|^2\hat{\chi}_k dt + \sqrt{\lambda_k} d\hat{W}_k. \tag{11}$$

where λ_k is the energy for Fourier mode k and $\hat{W}_k$ is a sequence of Brownian motions. The solution to this can be obtained exactly as

$$\hat{\chi}_k(t) = \hat{\chi}_k(0)e^{-\nu|k|^2 t} + \int_0^t \sqrt{\lambda_k} e^{\nu|k|^2(s-t)} d\hat{W}_k(s) \tag{12}$$

From the theory of stochastic integration (*29*) the integral in Eqn. 12 is a Gaussian process with mean zero and variance given by

$$\lambda_k \int_0^t e^{2\nu|k|^2(s-t)} ds = \frac{\lambda_k}{2\nu|k|^2}\left(1 - e^{-2\nu|k|^2 t}\right). \tag{13}$$

Each Fourier mode of χ can now be evolved in discrete time steps from a given initial condition by the formula

$$\hat{\chi}_k(t+\Delta t) = \hat{\chi}_k(t)e^{-\nu|k|^2\Delta t} + \sqrt{\frac{\lambda_k}{2\nu|k|^2}\,(1-e^{-2\nu|k|^2\Delta t})}Z_k \tag{14}$$

where Z_k are random numbers sampled from a $N(0,1)$ distribution but again subject to the complex conjugate constraint $Z_k = Z^*_{-k}$. We take as an initial condition the steady state by letting $t \to \infty$ and sampling according to the uncorrelated variance.

1.6 Data processing and tracking

All image processing was performed on the infrared video footage within `Matlab`. First we averaged pixel values over two consecutive frames of the video to remove noise and then subtracted a background image of the empty arena. Next we thresholded the image to a binary map, each pixel being 0 (no fish) or 1 (contains fish). To calculate performance we averaged the light level at each pixel containing fish.

To obtain fish trajectories we used `regionprops` to identify connected clusters of pixels with a value of 1 – each of these patches was a potential fish. We discarded any patches that were less than 60 pixels and took the centroids of the remaining patches to be the positions of the fish. To arrive at a threshold of 60 pixels, we used the algorithm outlined above on several sections of video, and determined manually which patches were fish, by comparing them to the original footage. The typical fish was about 30 pixels long and 4 wide, for an area of 120 pixels. To be conservative we used half that value as the threshold. Next the positions at each time step were linked to form trajectories. Continuous trajectories were obtained for all group sizes excluding 256. For this group size the frequency of occlusions meant accurate trajectories could not be obtained using our tracking software.

Positions were linked across frames by firstly making an Euler prediction of next position based on velocity and current position. The predicted position was then compared to the actual

measured positions at time $t+1$ and a Bertsekas auctioning algorithm (*30*) was used to link the measured positions across time frames. This algorithm proceeds as follows, We aim to match measurement $m_{i,t}$ taken and time t with measurement $m_{j,t+1}$. To do this we define a benefit a_{ij} associated with the asignment of $m_{i,t}$ to $m_{j,t+1}$ that is a function of the distance between the prediction for $m_{i,t}$ and the actual location $m_{j,t+1}$. We then seek a one-to-one assignment between each $m_{i,t}$ and $m_{j,t+1}$ such that the total benefit $\sum_{i=1}^{N} a_{ij}$ is maximized. To find this mapping the algorithm outlined in (*30*) is used.

We refer to each measurement $m_{i,t}$ as a bidder and each $m_{j,t+1}$ as an object that begins with a randomly assigned price, and is initially allocated to a bidder also at random. Each bidder has a level of satisfaction which is $a_{ij} - p_j$, that is the benefit of being assigned object j minus the cost of that object. The bidder is assumed to be sufficiently satisfied if

$$a_{ij} - p_i \geq \max\left(a_{ik} - p_k\right) - \epsilon \tag{15}$$

i.e. the bidder will not improve by more than ϵ by switching to a different object. Dissatisfied bidders are select at random, they choose the object that maximizing their satisfaction level, then trade objects with its current owner. The price of the object is then set to the maximum the new owner is prepared to pay, that is the exact price above which the bidder would rather switch to another object. This process continues until all bidders are within the range ϵ of being maximally satisified (see (*30*) for a discussion of convergence, optimality and the role of ϵ for this algorithm).

1.7 Individual-based zonal model

To test whether collective gradient tracking could emerge from the differential speed algorithm we observed the fish using, we employed a canonical schooling model (*17*). In this model agents tend to be attracted to and orientate their headings with nearby neighbors, while avoiding collisions.

Each individual with position vector $\mathbf{c}_i$ and direction vector $\mathbf{v}_i$ attempts to maintain a minimum distance r_r between itself i and others j at all times by turning away from any neighbors within a radius of repulsion, r_r. If any neighbors are present within this radius, the focal individual experiences a force of repulsion, and moves in a direction defined by,

$$\mathbf{d}_r(t+\Delta t) = -\sum_{j\neq i}^{n_r} \frac{\mathbf{c}_j - \mathbf{c}_i}{|\mathbf{c}_j - \mathbf{c}_i|}. \tag{16}$$

Repulsion has the highest priority, so if $n_r > 0$ the desired direction for the i^{th} individual is solely determined by repulsion: $\mathbf{d}_i(t+\Delta t) = \mathbf{d}_r(t+\Delta t)$.

If there are no neighbors within the radius of repulsion the focal individual will tend to orient with all n_o neighbors within its radius of orientation, r_o.

$$\mathbf{d}_o(t+\Delta t) = \sum_{j=1}^{n_o} \frac{\mathbf{v}_j}{|\mathbf{v}_j|} \tag{17}$$

It will also be attracted towards all n_a neighbors within its radius of attraction, r_a.

$$\mathbf{d}_a(t+\Delta t) = \sum_{j\neq i}^{n_r} \frac{\mathbf{c}_j - \mathbf{c}_i}{|\mathbf{c}_j - \mathbf{c}_i|} \tag{18}$$

The net social force will then be an equal normalized combination of orientation and attraction, $\mathbf{d}_i(t+\Delta t) = \frac{1}{2}[\mathbf{d}_o(t+\Delta t) + \mathbf{d}_a(t+\Delta t)]$. If one of either n_o or n_a is zero $\mathbf{d}_i(t+\Delta t)$ is given solely by the other. If they are both zero $\mathbf{d}_i(t+\Delta t) = \mathbf{v}_i(t)$. Finally some noise is added to $\mathbf{d}_i(t+\Delta t)$ by rotating it by an angle taken at random from a circularly wrapped Gaussian distribution with standard deviation, σ. At each time step individuals rotate their heading towards $\mathbf{d}_i$ up to a max turning angle, θ. They then proceed in that direction the distance $|\mathbf{v}_i|\,\Delta t$.

We simulated the dynamics of these agents within the same light fields we presented to the fish. The particles in this model had no gradient sensing capability, however, motivated by Figure 2A, they measured their current local light level, l_i, and modified the speed at which they

moved, $|\mathbf{v}_i|$, according to,

$$|\mathbf{v}_i| = V_{min} + l_i(V_{max} - V_{min}) \tag{19}$$

That is, we varied the speed linearly with local light level. The direction of their movement was purely social and was determined from the equations above using the parameters in Table S2. For the simulations, the schooling groups were placed in a periodic square domain of length 160cm.

1.8 Individual-based topological model

To further show the generality of our result we also implemented a topological interaction model (*18*). In this model, as in the zonal model, each individual attempts to maintain a minimum distance r_r between itself i and others j by turning to the direction defined by,

$$\mathbf{d}_r(t + \Delta t) = -\sum_{j \neq i}^{n_r} \frac{\mathbf{c}_j - \mathbf{c}_i}{|\mathbf{c}_j - \mathbf{c}_i|}. \tag{20}$$

If there are no neighbors within this zone the focal individual will interact with its m nearest (or topological) neighbors,

$$\mathbf{d}_i(t + \Delta t) = \sum_{j \neq i, j \in \mathcal{N}} \left(\frac{\mathbf{c}_j - \mathbf{c}_i}{|\mathbf{c}_j - \mathbf{c}_i|} + \frac{1}{3} \frac{\mathbf{v}_j}{|\mathbf{v}_j|} \right) \tag{21}$$

where $\mathcal{N}$ is the topological neighborhood and the orientation vector is given one third of the weighting as the attraction vector. Following (*18*), and to ensure the groups remain cohesive, we employ a spatially balanced model so that $\mathcal{N}$ is defined as the neighborhood consisting of the $m/2$ nearest neighbors situated within an angle between $-2\pi/3$ radians and 0 radians of the focal individual (relative to its current orientation), the $m/2$ nearest neighbors located at an angle between 0 radians and $2\pi/3$ radians, and no neighbors that are located outside of these two regions (i.e. neighbors located to the rear of the focal individual).

Again individuals were simulated within the light fields presented to the fish and their speed was controlled according to Eqn 19.

2 Supplementary Text

2.1 Parameter scans

In addition to the results shown in Figure 1B of the main text, we also show the behaviour of the zonal numerical schooling model, described in Section 1.7, over a larger region of parameter space. As shown in Figure S4 the qualitative increase in performance with increasing group size exists over a wide range of parameter space. Further, there is a substantial region in parameter space which exhibits the same quantitative pattern as found in our experiments (region around dashed line in Figure S5). While we stress that the simple interaction models we employ are over-simplifications of the behavior of real fish, these results represent a proof-of-principle that the underlying mechanism we describe will lead to enhanced gradient tracking performance.

The sensitivity of the behavior of the numerical model to the strength of the light-dependent speed function was also investigated. Figure S7 shows in the gradient tracking performance of the numerical model versus group size for various values of the maximum speed (the speed that corresponds with the brightest light level). The qualitative trend matched that of the experiment for all curves over the range of maximum speeds we used, though the performance gain increased monotonically with increasing maximum speed.

2.2 Results of individual-based topological model

To highlight the generic nature of the emergent gradient tracking mechanism, we simulated groups, again exhibiting a light speed relationship, but using topological based social interaction rules as described in Section 1.8. Figure S8 shows the gradient tracking performance as a function of group size for these simulations with various number of topological neighbours. As in the zonal model and experimental data, larger groups track the dark patch more effectively. For the topological model we observe a dip in performance at intermediate group sizes as we found these groups exhibit relatively stationary, and disordered, swarm-like behavior and thus

perform worse than an individual which moves thoughout the domain yet slows when it is in favorable areas.

2.3 Group size and length scale

To investigate the key drivers of the increased performance for larger groups in the numerical models, we rescaled the effective size of an individual so that the relative length scales of the environment and the group could be varied independently. By scaling all radii of interactions between individuals while keeping their ratios fixed, we effectively alter the size of an individual, or equivalently we alter the length-scale of the environment (light field), while keeping individual size constant. Figure S9A shows the performance versus group size (number of individuals in group) for various values of this individual size scaling. In Figure S9B we plot the same data but against the length scale of the group. To estimate this length scale we firstly assume the density of the group is defined as

$$\rho = 1/\pi r_r^2 \tag{22}$$

The area the group spans is then N/ρ and we take as a length scale the radius of the circle that would enclose this area. This radius is given by $r_r\sqrt{N}$.

We observe that a larger relative length scale is the primary driver of increased performance, and that above a certain length scale increasing group size can decrease tracking ability. However, for a fixed group length scale, groups with more individuals (lower scaling values) tend to do better. This shows that the cardinality of the group also plays a role. In short, the increased spatial extent of larger groups allows them to capture more variation in cue level, but the increase in numbers allows them to measure that variation more accurately.

2.4 Group turning due to variation in speed

In Figure 2A of the main text we see that individuals tend to move more quickly in brighter areas. We hypothesize that this leads to emergent group level gradient tracking since differential speeds combined with social forces will steer the group toward its slower side. It is therefore necessary to show that instantaneous differential speeds within the group cause turning.

To characterize the speed differential of a group we measure their speed as a function of their spatial coordinates on the $x - y$ plane. To this data we fit a linear 2D surface using least squares. We take the direction of steepest descent on this surface to be the direction from the centroid of the group toward its slowest region. At each time step we correlate this direction with the acceleration of the group, i.e. the direction in which the group turns. This correlation, averaged over time, is positive for our data; thus groups tend to turn towards their slower side. In Figure S10 we plot the correlation between the direction of acceleration of a group and the direction of the decrease of speed across the group (solid red line) as a function of group polarity. Group polarization, a measure of alignment, ranging from 0 for a disordered group, to 1 when all are fish moving in the same direction, is calculated as

$$\text{group polarization} = \frac{1}{N}\left|\sum_{i=1}^{N}\frac{\mathbf{v}_i}{|\mathbf{v}_i|}\right|, \tag{23}$$

where $\mathbf{v}_i$ is the velocity of the i^{th} fish and N the number of fish. We find that when the group is moderately polarized, variations in speed among individuals results in turning towards those who move more slowly (Figure S10).

To separate this effect from individuals turning towards darkness, which will also tend to be in the direction of the slower side of a group, we perform a similar analysis using light level. This time we use light level as the z-axis and again fit a linear 2D surface. The direction of steepest descent on this surface is taken to be the direction of the darker side of the group. Just as before, we find the correlation between this direction and the direction of acceleration of

the group averaged over time. As shown by the solid blue line on Figure S10, this correlation is positive, demonstrating that groups do move towards the darkness, but that the influence is weaker than that resulting from the differential speed effect. Further, we look at these two measures when the two effects are in conflict, i.e. when the direction toward the slower side of the group points away from the darker side of the group (Figure S10, dashed lines). Turning due to differential speeds dominates, demonstrating that it is differential speed, not response to the dark directly, that produces turning. This in combination with the fish slowing in darker areas (Figure 2A), is the mechanism that results in the observed emergent taxis.

Figure S10 shows that the turning due to differential light is weaker than turning due to differential speeds, for all but extreme values of polarization. The lack of difference at high and low polarization is due primarily to group size effects; high values of polarization are dominated by small group sizes, which show a statistically weaker response to either variable. Low values of polarization, in general, characterize a stationary swarm state, in which individuals are often motionless and thus would not respond to either factor.

3 Supplementary figures

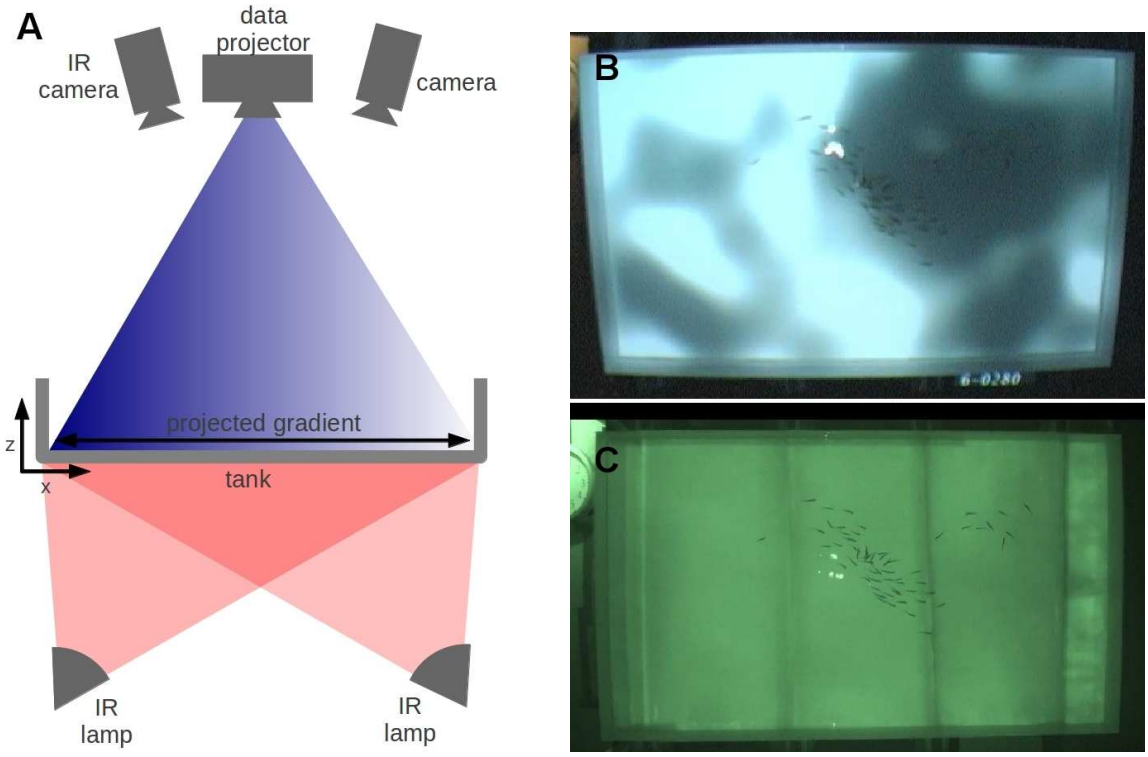

Figure S1: (A) Schematic of the experimental set-up. We project a light gradient on to a large shallow tank from above. We also illuminate the floor of the tank from below with infrared light and film from above with both visible and IR cameras. Snapshots from both cameras are shown in the right panel (B visible, C infrared). As golden shiners are highly cryptic when in the dark regions of the tank, we use the IR footage to obtain positions and trajectories for the fish. This likely forms the basis for their innate preference for these regions as, in their natural habitat, the threat of aerial predation will be stronger when light intensity, and thus contrast with the background, is high.

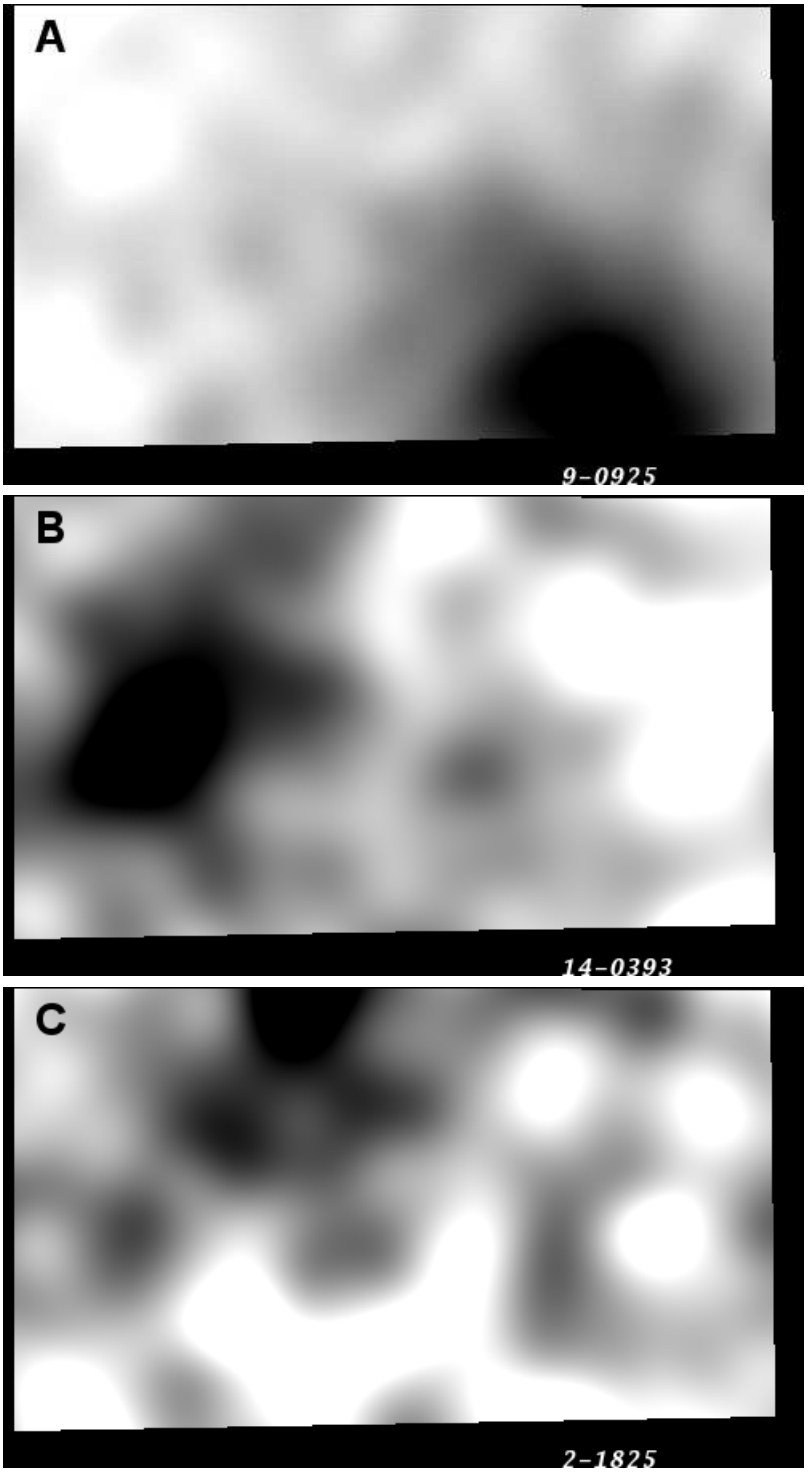

Figure S2: Examples of the different noise values used, (A) low, (B) medium and (C) high (0.1, 0.25 and 0.4).

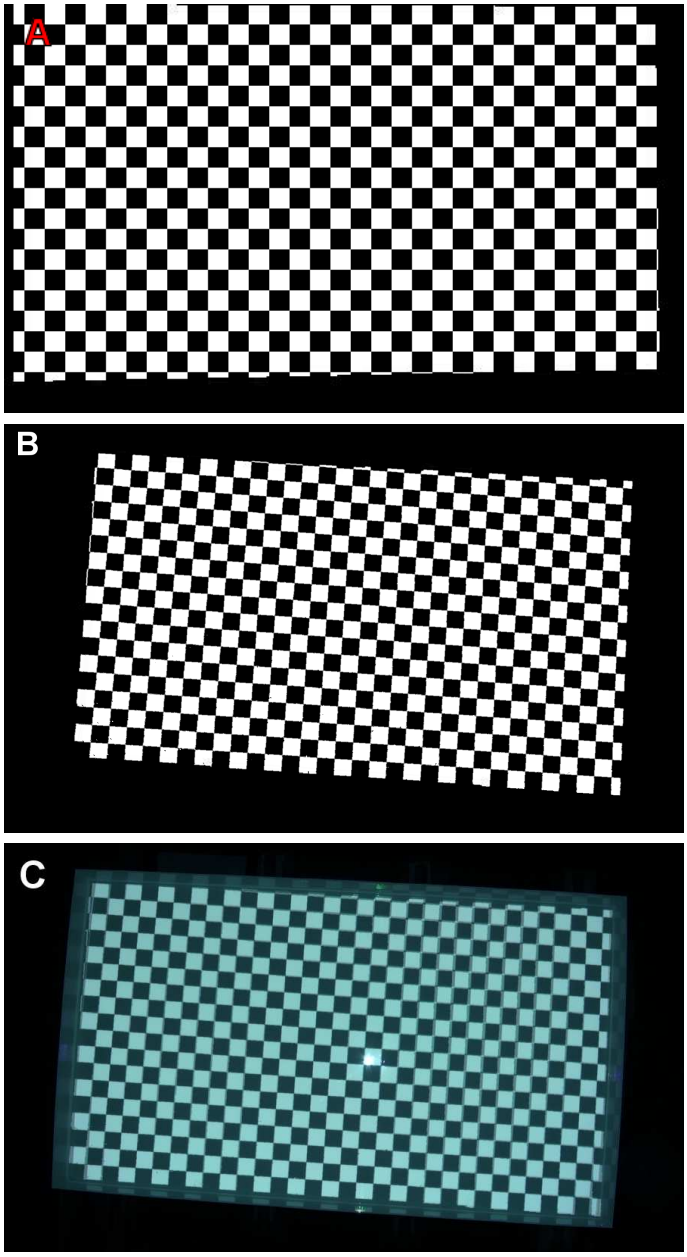

Figure S3: Calibration of projected image. To convert from the image space to real space a calibration image was projected onto the tank. The projected image was rescaled and transformed in three dimensional coordinates to account for parallax and distortion from the projector. The light level of the projected image could then be used to determine local levels experienced by the fish. (A) projected image, (B) transformed image, (C) superposition of transformed image with single frame from the camera.

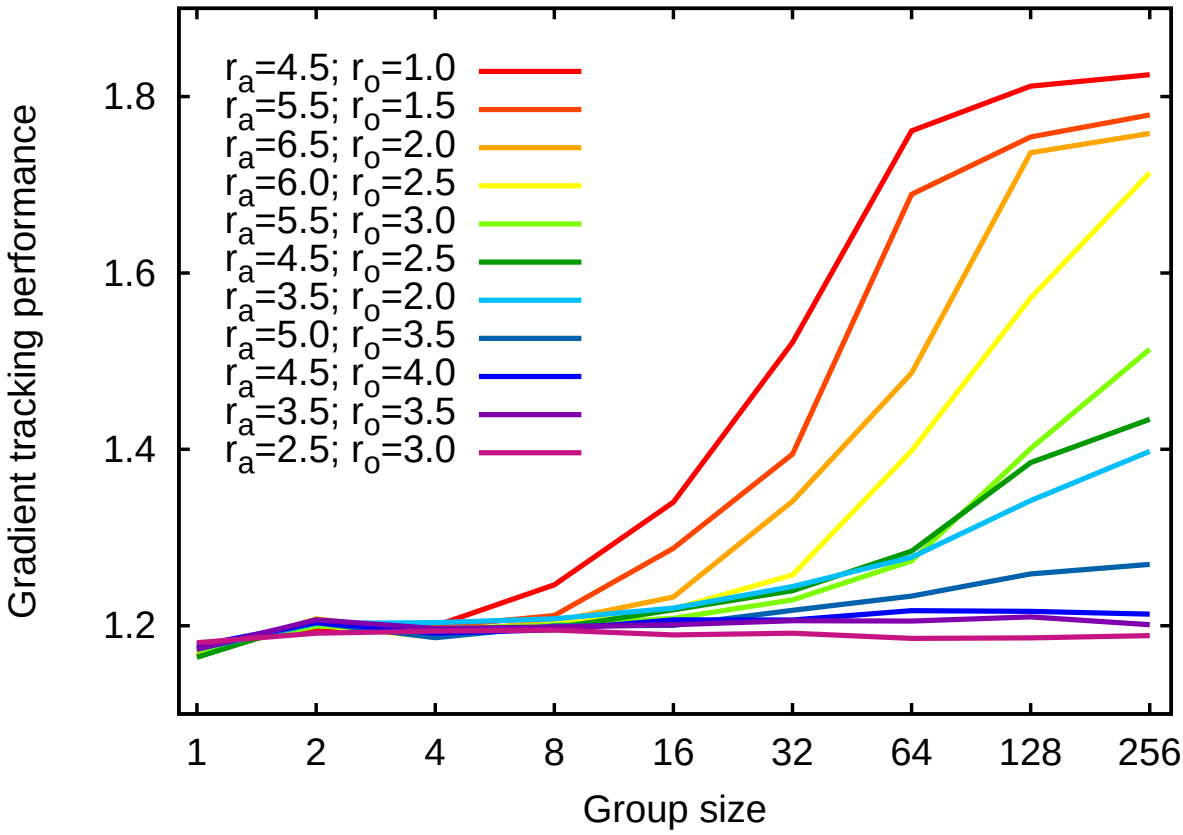

Figure S4: Numerical data: Gradient tracking performance of zonal schooling model as a function of group size. Different curves correspond to various combination of the radius of attraction, r_a, and radius of orientation, r_o. The qualitative trend in performance versus group size trend is the same over a large range of parameter space. The simulations used in Figure 1B of the main text is $r_a = 5.5$, $r_o = 3.0$. See Section 1.7 for model details.

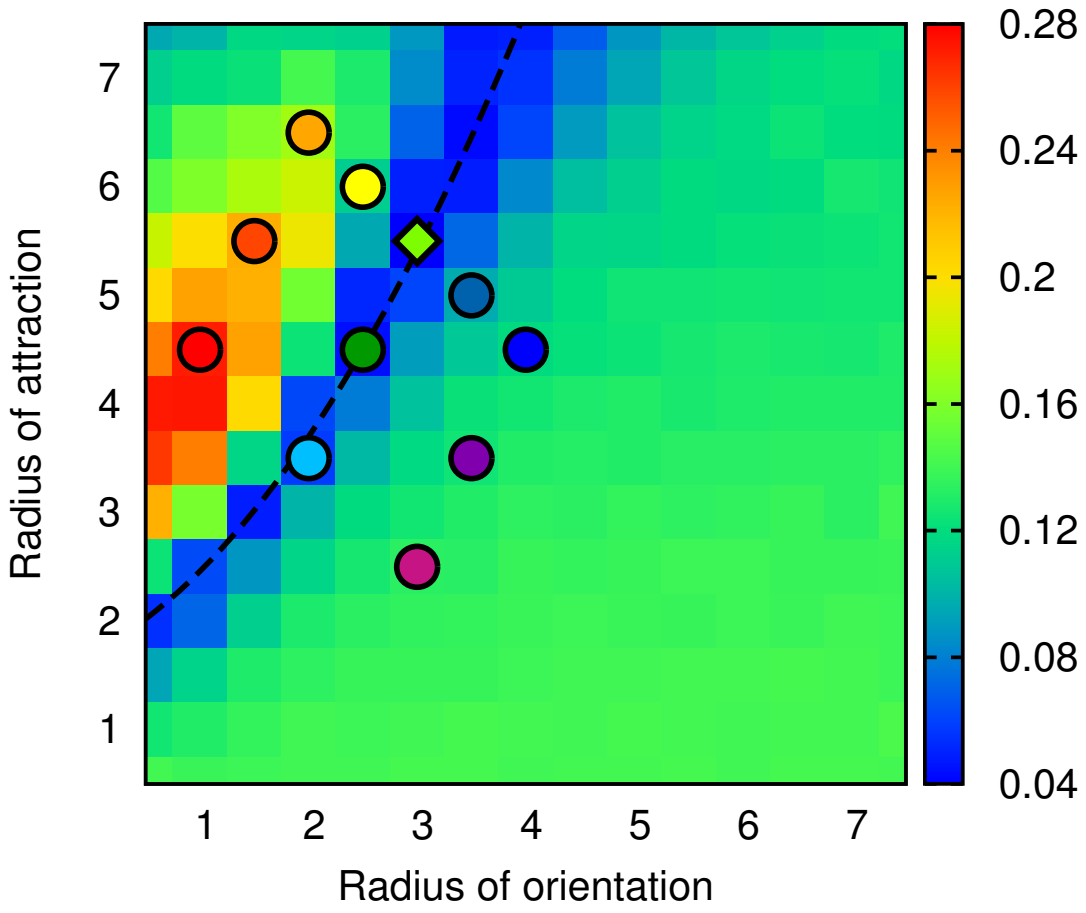

Figure S5: Numerical data: Root mean square error between performance of zonal schooling model and experimental data. Color symbols correspond to the curves in Figure S4 (matching colors). The diamond indicates the parameter values used in the simulations shown in the main text (Figure 1B). For the parameters in the band of blue area around the dashed black line, the quantitative performance of the model closely matches that of the experimental fish. See Section 1.7 for model details.

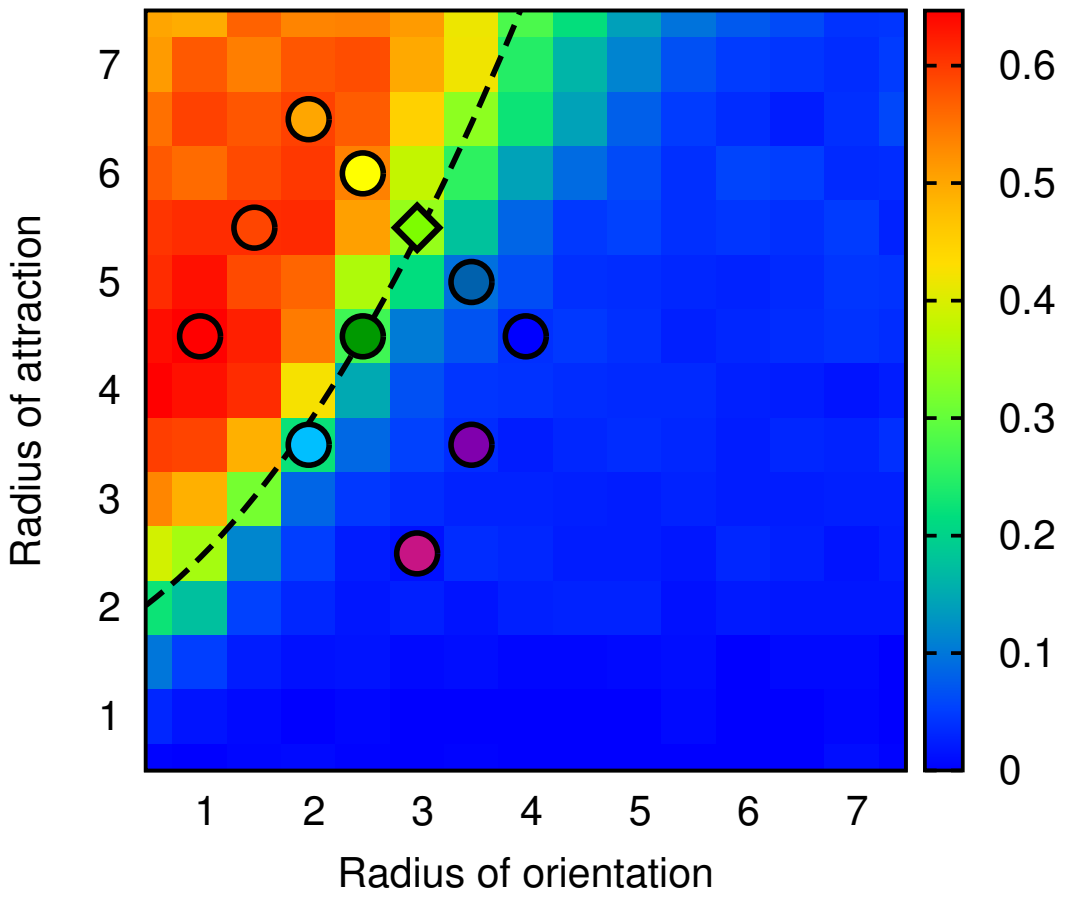

Figure S6: Numerical data: Maximum increase in performance as a function of model parameters. The color shows the difference between the performance of the highest performing group size and a single individual in the numerical model for a range of values of radius of attraction, r_a, and radius of orientation, r_o. The color dots correspond to the curves in Figure S4 with matching colors. The diamond corresponds to the parameter values used in the simulations shown in the main text. For a broad range of parameter space (area above the black dashed line) the model performs at least as well as the experimental data. See Section 1.7 for model details.

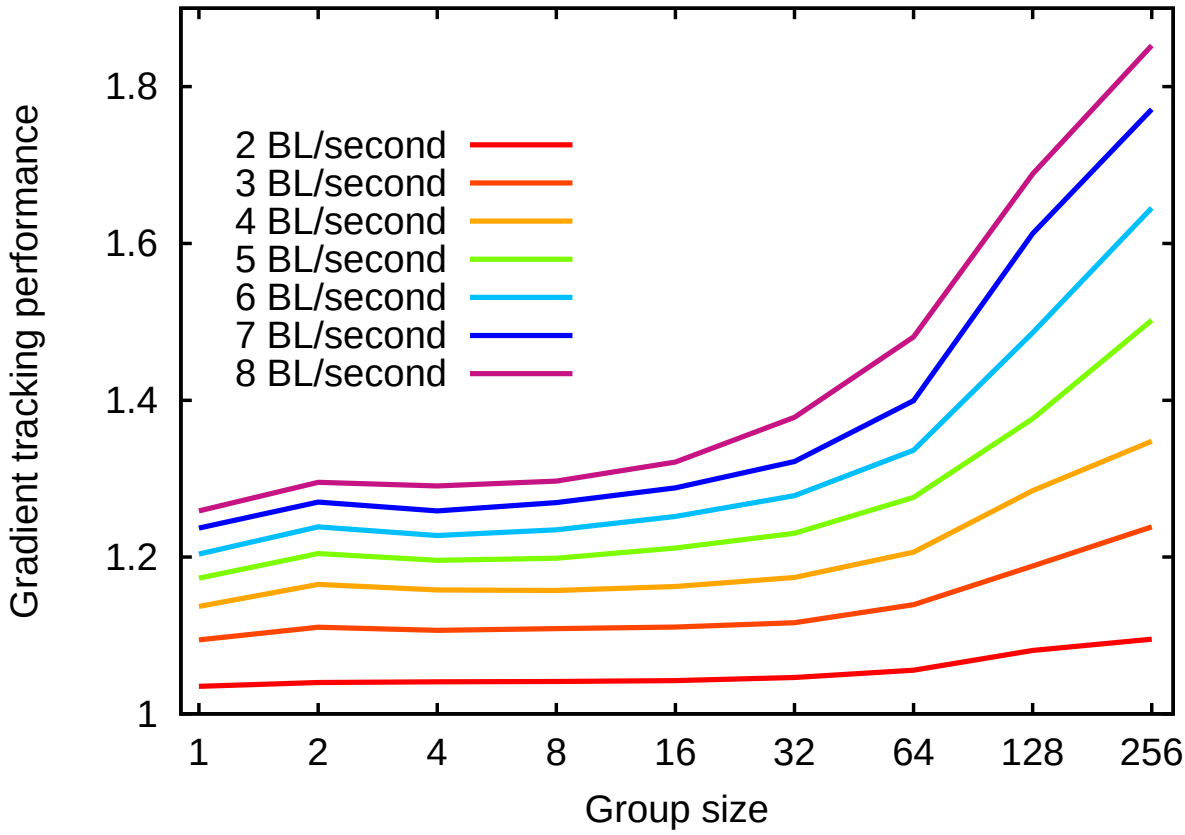

Figure S7: Numerical data: Gradient tracking performance of numerical schooling model (zonal) as a function of group size for different speed-light relationships. Curves correspond to various values of the maximum speed. For all curves the minimum speed was 0.5 body lengths per second. The simulations used in Figure 1B of the main text have a maximum speed of 5 BL/second.

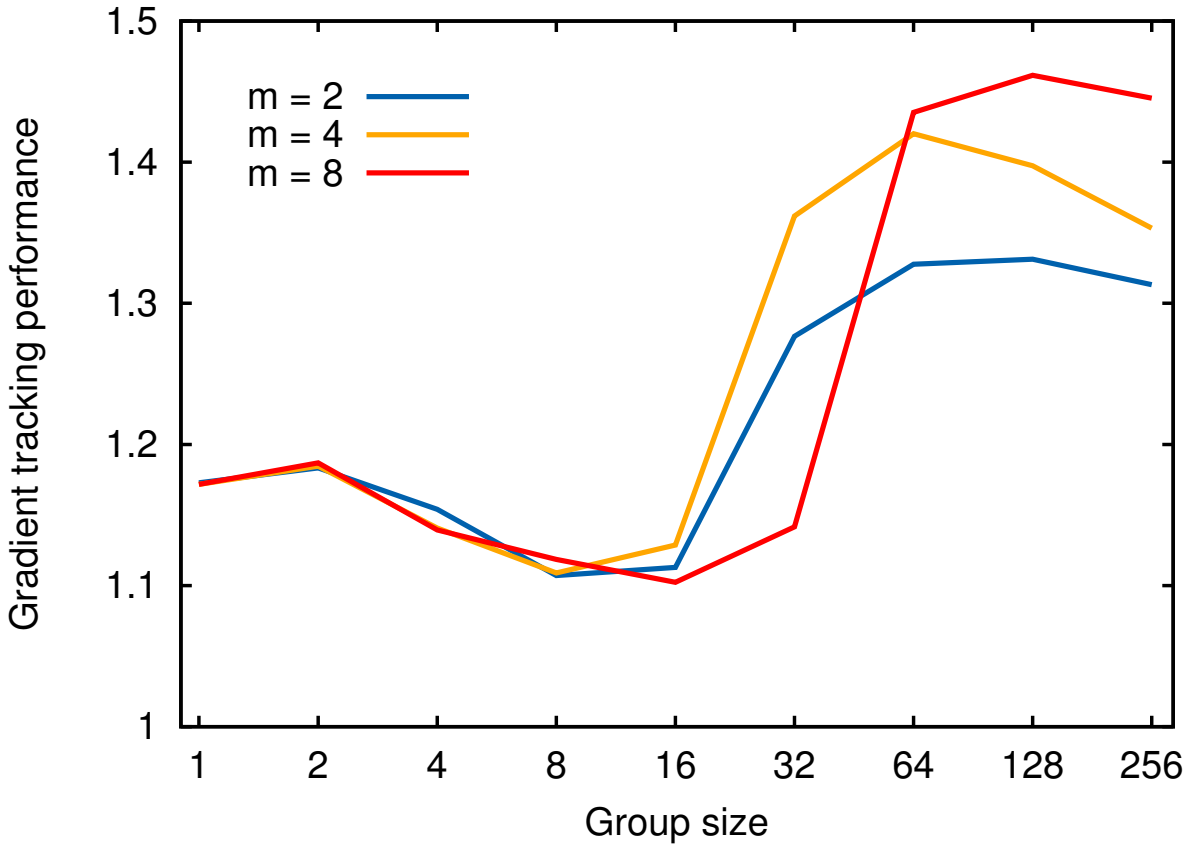

Figure S8: Numerical data: Gradient tracking performance of topological schooling model as a function of group size for different interaction neighborhoods. Curves correspond to various values of the number of topological neighbors that are interacted with. A performance dip is observed for intermediate group sizes as these groups tend to form less mobile swarms, and therefore perform worse than an individual that moves throughout the domain.

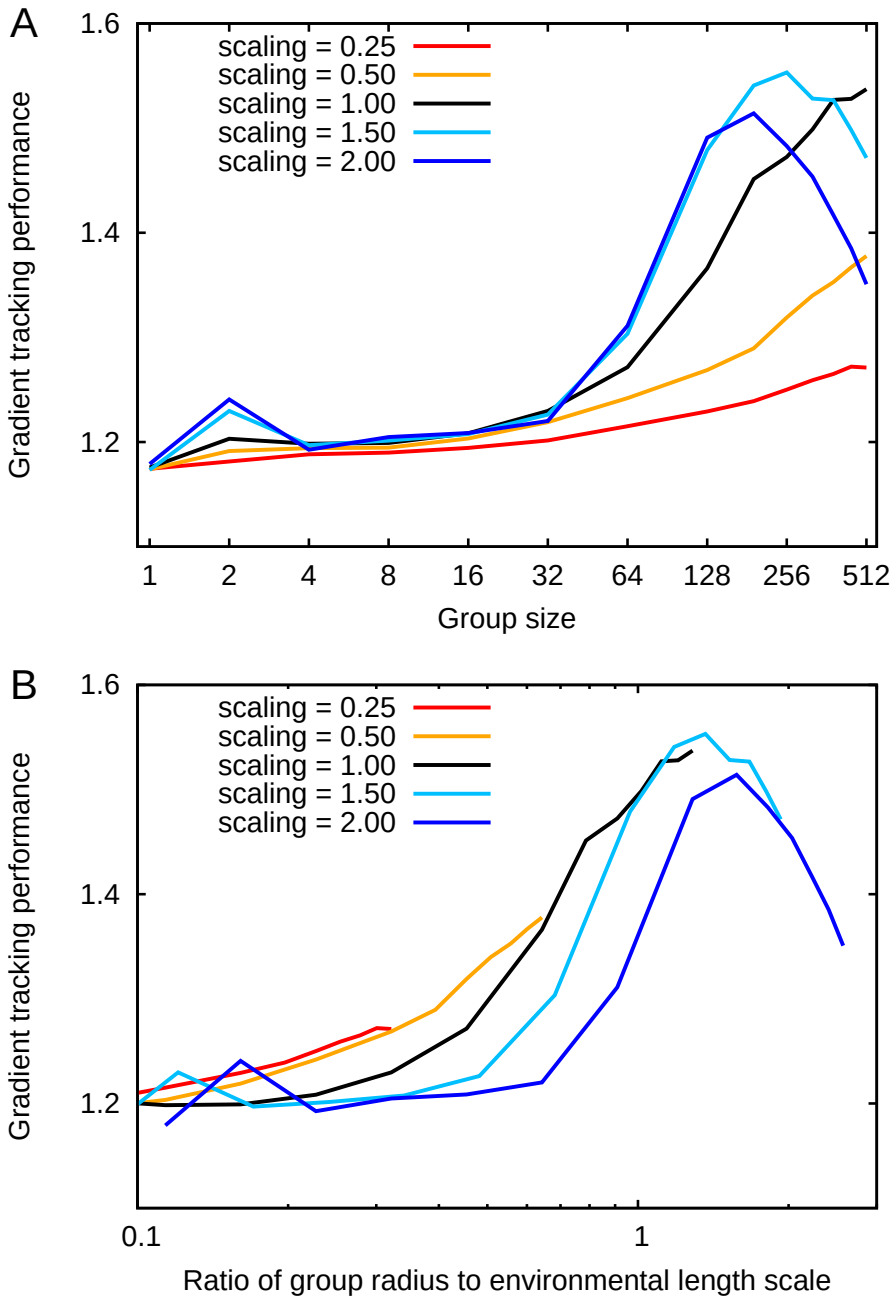

Figure S9: Numerical data: Gradient tracking performance of the zonal schooling model as a function of group size for different scalings of the interaction zones. In panel A the x-axis refers to the number of individuals in a group; at a given group size each curve has a different length scale (spatial size). In panel B the x-axis is the spatial size of the group, relative to the length scale of the environment; at a given value of the x-axis each curve has the same spatial size, but a different density (lower scaling value means higher density). The most dramatic increase in performance occurs when the length scale of the group approaches the characteristic length scale of the environment (1 on the x-axis).

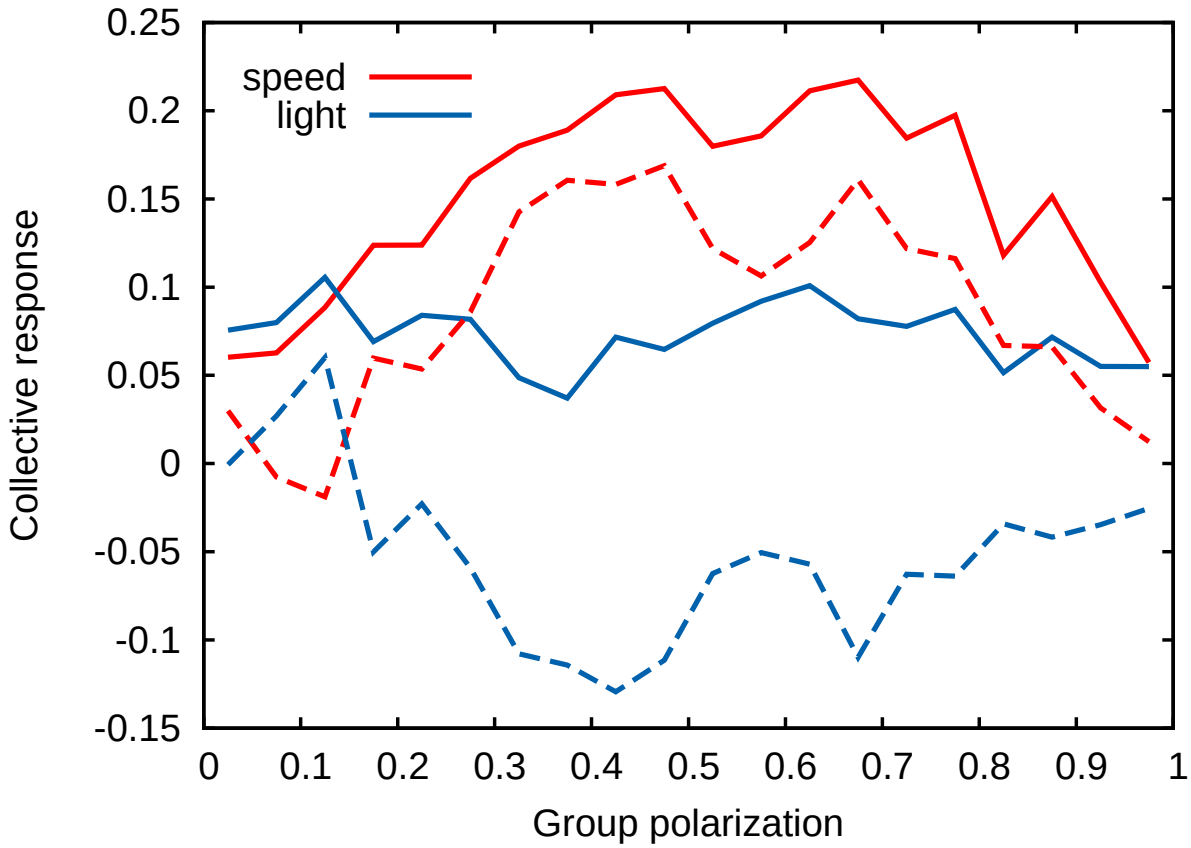

Figure S10: Experimental data: Group turning response to differential speeds and light levels. The solid red line shows the correlation between the direction of acceleration of the group and the direction pointing towards the slow side of the group as a function of group polarization. The solid blue line shows correlation between the direction of acceleration and the direction pointing towards the darker side of the group. We see that, though positive, this turning due to differential light is weaker than turning due to differential speeds, for all but extreme values of polarization. Further, when we look at these same quantities when the direction of the slow side of the group and the direction of the dark side of the group are opposite i.e. when these two turning mechanisms are in conflict (dashed lines), we see that for most levels of polarization the effect from speed dominates. Turning due to differential speeds (towards the slower side of the group) is the stronger steering mechanism. See Section 2.4 for details of calculations.

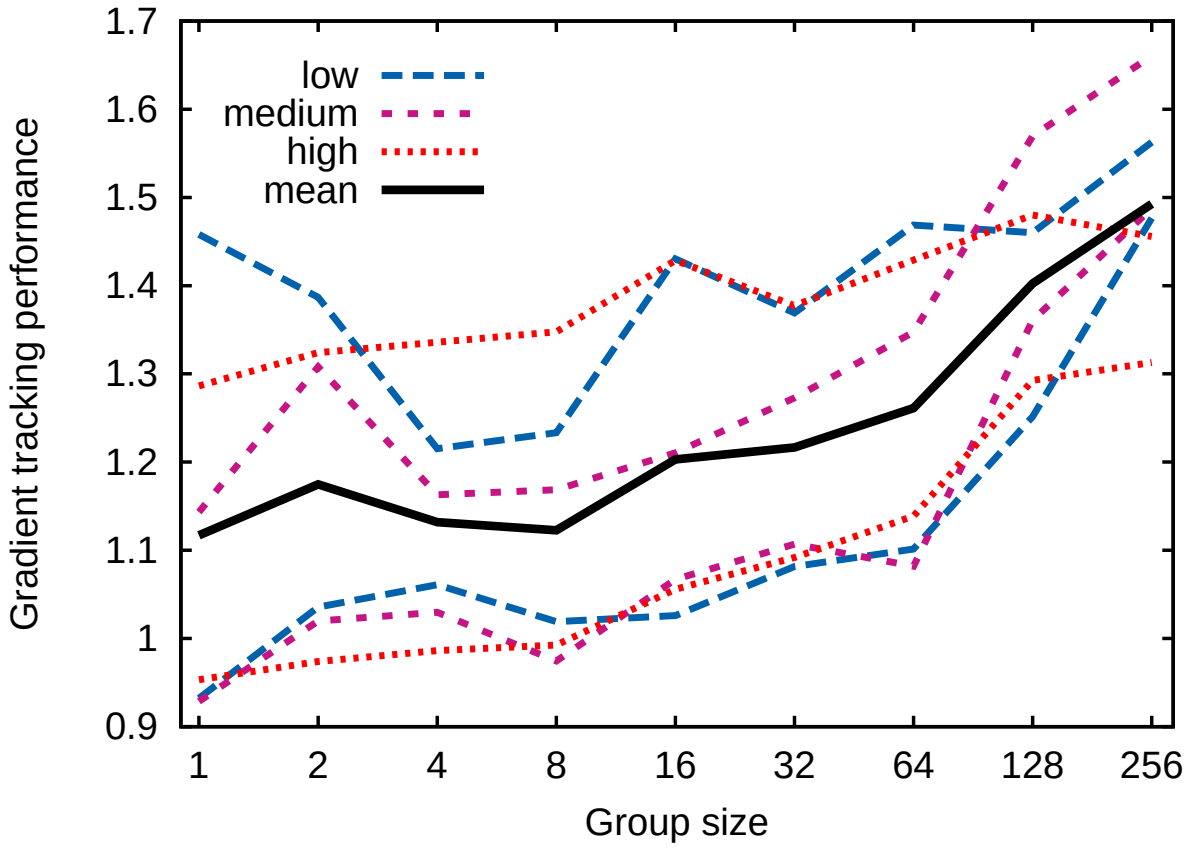

Figure S11: Experimental data: Performance as a function of noise. Broken lines of similar color and style show the upper and lower bounds of the standard deviation around the mean. Each noise level is a different color and line type. The solid black line is average over noises, and is also shown as points in Figure 1B of the main text. The level of noise in the light field had no significant effect on the gradient tracking performance.

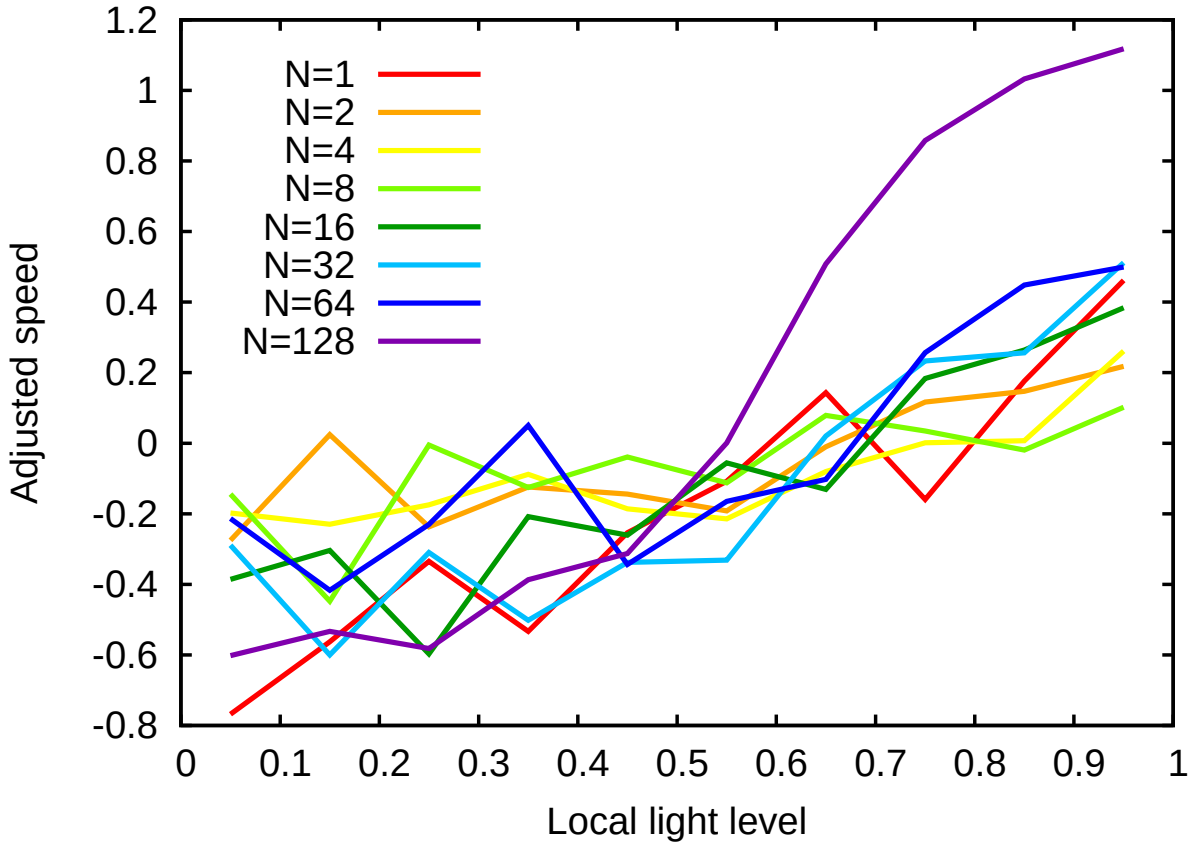

Figure S12: Experimental data: Average speed as a function of local light level, plotted separately for each group size. Fish in groups of all sizes and solitary fish tend to swim more quickly in brighter regions. The speed is adjusted to control for any correlation between speed and spatial use patterns not dependent on the light fields - see Section 1.3 for details. Speed values shown are averaged across measurements taken once every 3 seconds from a single randomly selected fish to avoid temporal and spatial autocorrelation. For each group size data is averaged over noise levels.

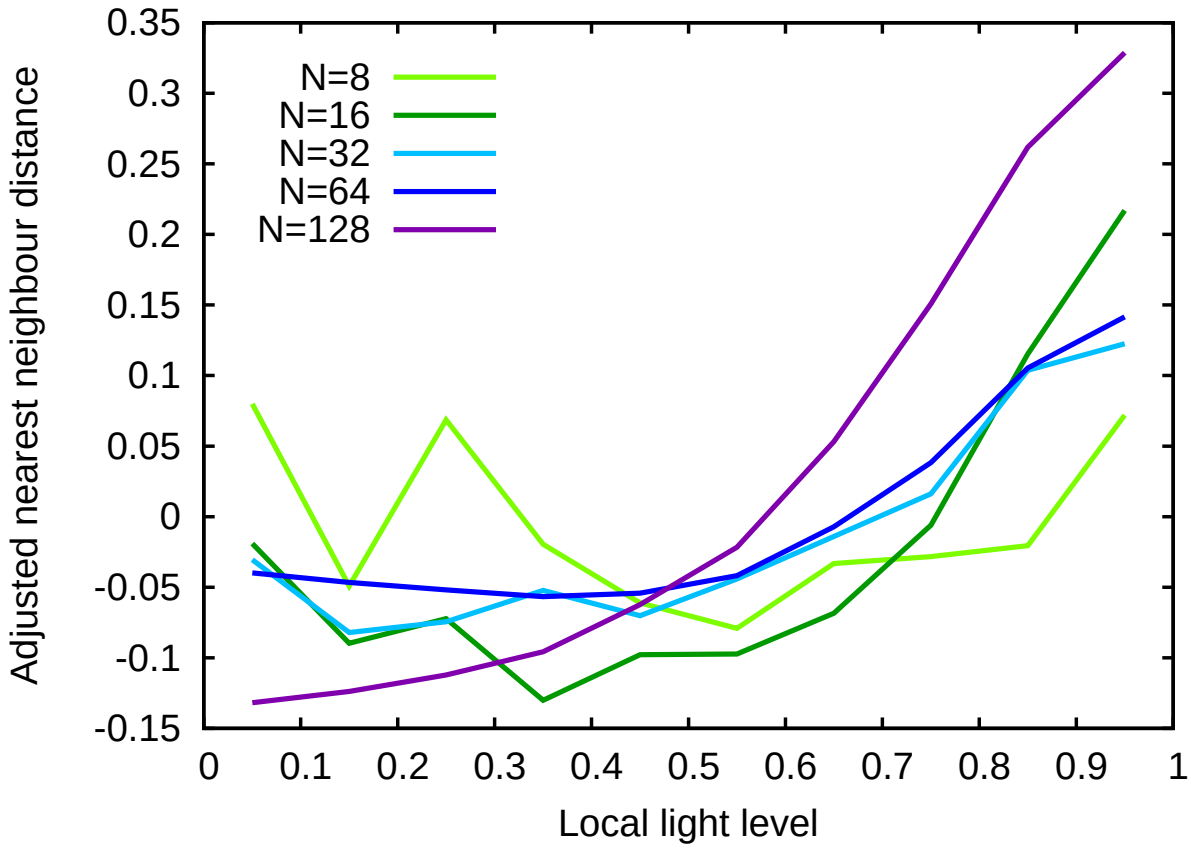

Figure S13: Experimental data: Average distance to nearest neighbor as a function of local light level, plotted separately for each group size. Across group sizes, the average distance between a focal fish and its nearest neighbor increases with increasing brightness. Therefore schools tend to be denser in darker areas. We have adjusted the distance, to control for any correlation between density and spatial use patterns not dependent on the light fields - see Section 1.3 for details. Nearest neighbor distances shown are averaged across measurements taken once every 3 seconds from a single randomly selected fish to avoid temporal and spatial autocorrelation and then averaged across group sizes 8 to 128 and all noise levels. We have restricted this analysis to group sizes of at least 8 as smaller group sizes did not yield sufficient data. Distance is measured in body lengths.

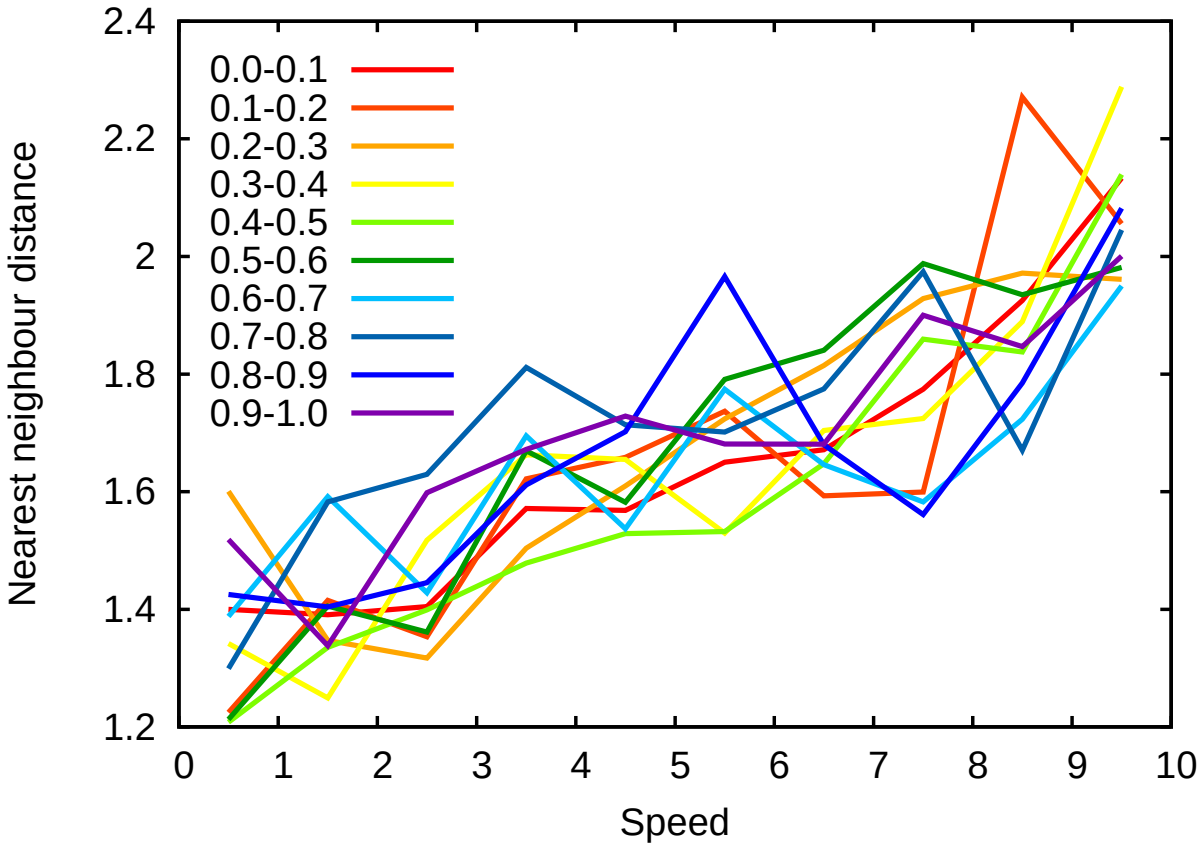

Figure S14: Experimental data: Average distance to nearest neighbor as a function of speed. Each curve shows data for fish at a certain local light level, (see legend for light values). Across local light levels, the average distance between a focal fish and its nearest neighbor increases with increasing speed. This trend is independent of light level, meaning the fish regulate their inter-individual spacing according to their speed. For each light level data is averaged over group sizes and noise levels. Speed values shown are averaged across measurements taken once every 3 seconds from a single randomly selected fish to avoid temporal and spatial autocorrelation and then averaged across group sizes 8 to 128 and all noise levels. Distance is measured in body lengths and speed in body lengths per second.

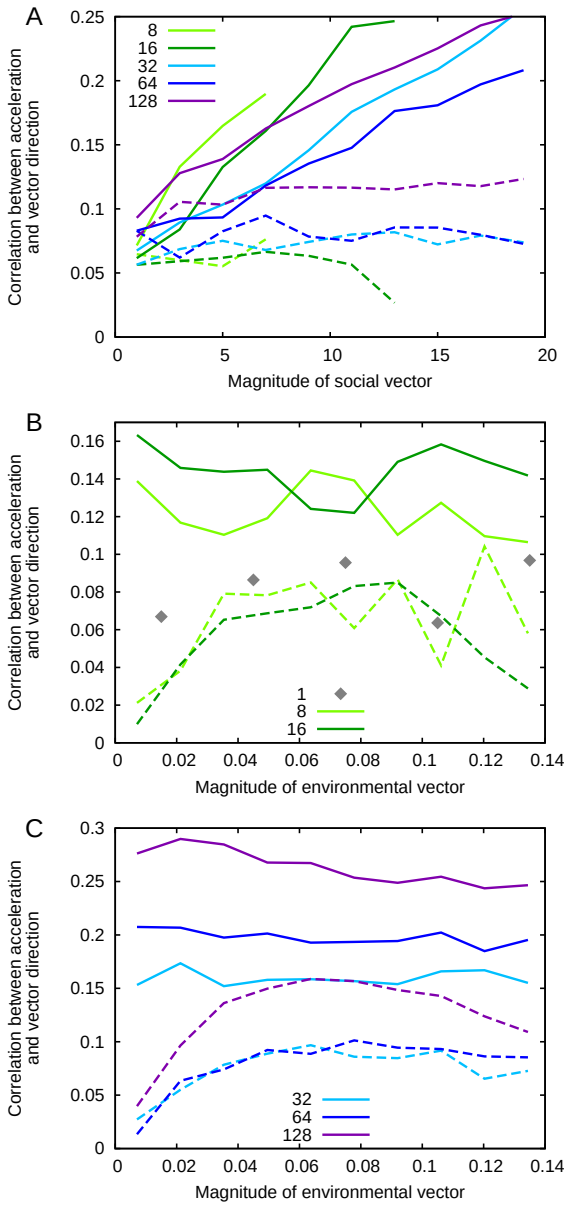

Figure S15: Experimental data: Individual response to local light gradient and social vector, plotted separately for each group size. (A) Solid lines show acceleration toward near neighbors (within 7 body lengths) as a function of the length of the social vector (Eqn. 2). Broken lines show acceleration in the direction of the local light gradient. (B-C) Individual response to neighbors and light gradient as a function of the magnitude of the local light gradient. Turning response to social vector (solid lines) consistently dominates the influence of the local light gradient (broken lines). For each group size data is averaged over noise levels.

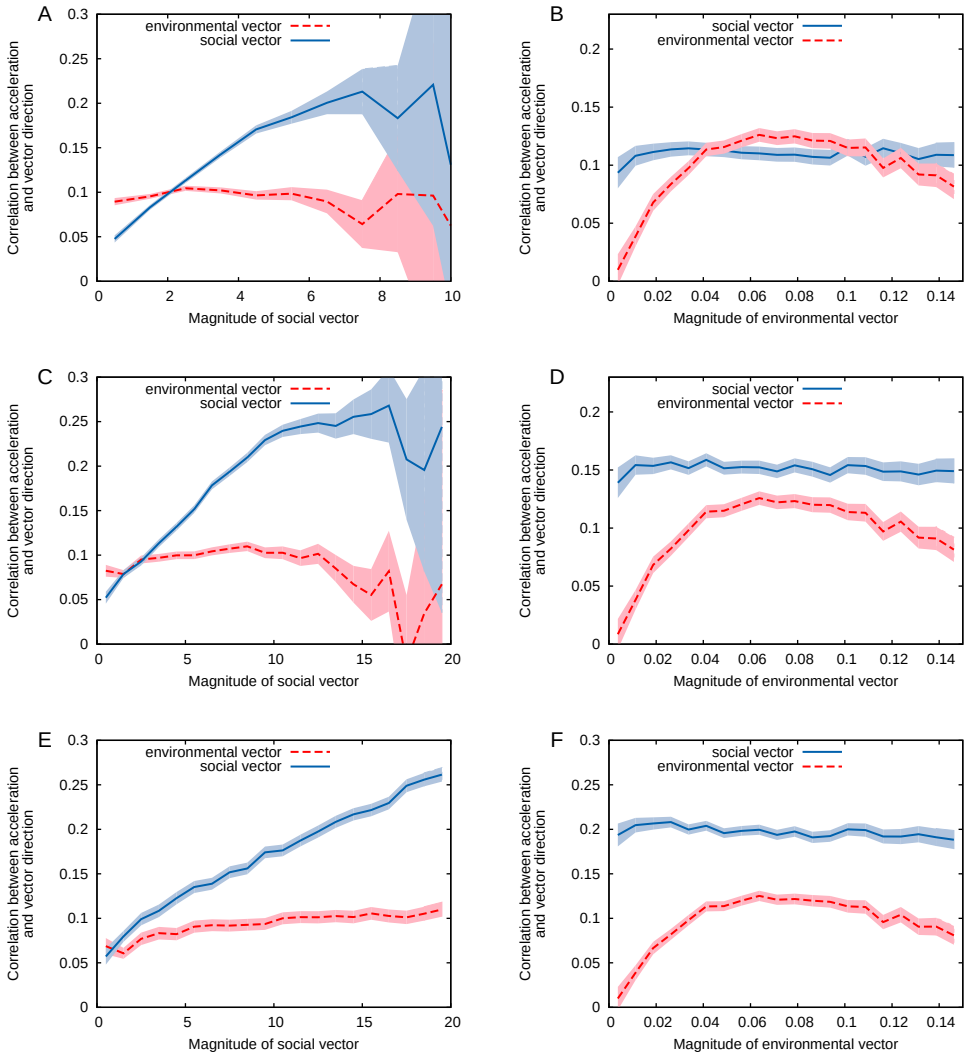

Figure S16: Experimental data: Individual response to social and environmental cues as a function of the magnitude of the social vector, $|\mathbf{S}|$. (A,C,E), and of the magnitude of the environmental vector, $|\mathbf{G}|$ (B,D,F). Different interaction ranges are assumed when calculating social correlation the measure. (A-B) 3 body lengths, (C-D) 5 body lengths, (E-F) 9 body lengths. In all other respects these figures are equivalent to Figures 2B and 2C of the main text.

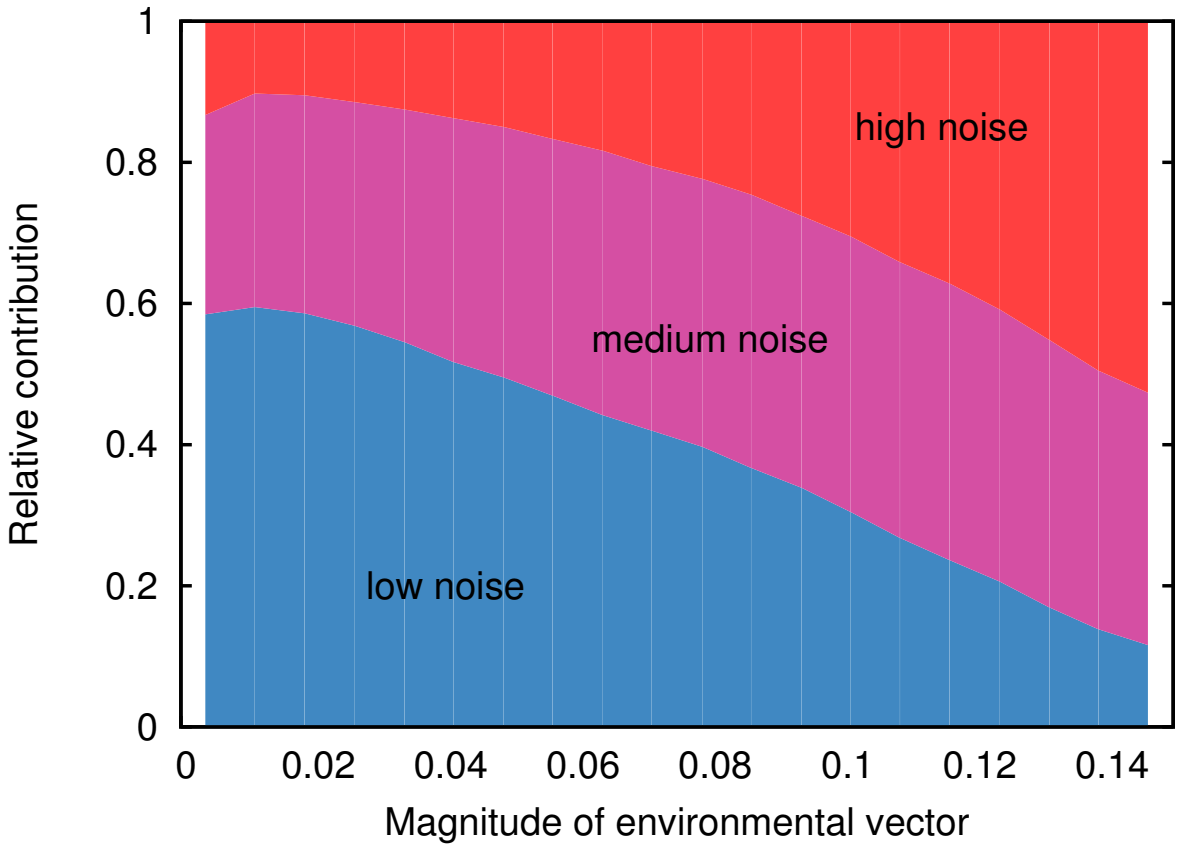

Figure S17: Experimental data: Relative contribution from each noise level to the curve shown in Figure 2C of the main text. Figure 2C shows the individual response to the environmental vector as a function of the magnitude of the environmental vector, $|\mathbf{G}|$, averaged over noise levels. For high magnitudes of this vector we see a slight decrease in the average response. This dip occurs because such steep changes in light level (greater than 0.11) are contributed predominantly by local, ephemeral noise and not the longer-range feature to be tracked. When noise levels are high the spatiotemporal field dominates and we therefore see a larger contribution from the high noise level for the large magnitude gradients. For low noise levels, gradients are determined by the circular region and vector magnitudes are lower.

Table S1: Experimental schedule. Each combination of group size and noise level found in a row of the table represents 4 six-minute trials. The videos for group size 2 on day 8 and group size 64 on day 13 were corrupted (denoted by *) and consequently rerun on days 17 and 15 respectively.

Day	Group size	Noise
1	64, 32, 8, 16, 4, 2	medium
2	8, 2, 4, 64, 16, 32	low
3	64, 4, 2, 8, 32, 16	high
4	4, 64, 8, 2, 16, 32	high
5	16, 2, 64, 4, 32, 8	medium
6	8, 16, 4, 2, 32, 64	low
7	16, 4, 32, 8, 64, 2	high
8	2^*, 32, 64, 16, 8, 4	low
9	16, 4, 64, 32, 2, 8	medium
10	4, 2, 8, 16, 64, 32	medium
11	64, 32, 16, 4, 8, 2	low
12	32, 8, 16, 64, 2, 4	high
13	8, 64^*, 2, 32, 16, 4	medium
14	32, 64, 2, 4, 8, 16	high
15	32, 16, 4, 64, 2, 8	low
15	64	medium
16	128	medium, low, high
17	128	high, medium, low
17	2	low
18	128	low, high, medium
19	128	high, low, medium
20	128	low, medium, high
21	1	medium, low, high, high, medium
21	256	medium
22	1	low, high, low, medium, medium
22	256	high
23	1	low, high, medium, high, low
23	256	low

Table S2: Parameter values for generated light field, experimental arena and simulation model. Simulation values shown were used for simulation run shown in Figure 1B of main text.

Parameter	Domain		
	Image	Arena	Simulation
Tank length	-	213cm	160cm
Tank width	-	122cm	160cm
Tank area	-	2.6m^2	2.56m^2
Decay length of patch (D)	100 pixels	44.53cm	44cm
Speed of patch	8 pixels/s	3.56cm/s	3.52cm/s
Dominant wave number of noise (k_0)	24	-	16.84
Characteristic length scale of noise	67.02 pixels	29.84cm	29.85cm
Temporal autocorrelation of noise (ν)	0.001	-	0.001
Body length	-	4.9cm	5.0cm
Radius of repulsion, r_r	-	-	2.5cm
Radius of alignment, r_o	-	-	15cm
Radius of attraction, r_a	-	-	27.5cm
Max swim speed	-	-	25cm/s
Min swim speed	-	-	7.5cm/s
Direction update rate, $1/\Delta t$	-	-	8/s
Max turning rate	-	-	1.75 radians / update
Rotational noise, (σ)	-	-	0.01 radians

References

1. A. W. Woolley, C. F. Chabris, A. Pentland, N. Hashmi, T. W. Malone, Evidence for a collective intelligence factor in the performance of human groups. *Science* **330**, 686 (2010).

2. D. Grünbaum, *Evol. Ecol.* **12**, 503 (1998).

3. A. M. Simons, Many wrongs: The advantage of group navigation. *Trends Ecol. Evol.* **19**, 453 (2004).

4. E. A. Codling, J. W. Pitchford, S. D. Simpson, Group navigation and the "many-wrongs principle" in models of animal movement. *Ecology* **88**, 1864 (2007).

5. P. A. Larkin, A. Walton, Fish school size and migration. *J. Fish. Res. Board Can.* **26**, 1372 (1969).

6. C. W. Clark, M. Mangel, The evolutionary advantages of group foraging. *Theor. Popul. Biol.* **30**, 45 (1986).

7. I. D. Couzin *et al*., Uninformed individuals promote democratic consensus in animal groups. *Science* **334**, 1578 (2011).

8. N. R. Franks, S. C. Pratt, E. B. Mallon, N. F. Britton, D. J. Sumpter, Information flow, opinion polling and collective intelligence in house-hunting social insects. *Phil. Trans. R. Soc. B* **357**, 1567 (2002).

9. F. Galton, Vox populi. *Nature* **75**, 450 (1907).

10. S. Bauer *et al*., in *Animal Migration: A Synthesis*, E. J. Milner-Gulland, J. M. Fryxell, and A. R. E. Sinclair, Eds. (Oxford Univ. Press, New York, 2011), pp. 68–87.

11. T. J. Pitcher, J. K. Parrish, *Behaviour of Teleost Fishes* (Springer, New York, 1993), vol. 2, pp. 369-439.

12. R. Poli, J. Kennedy, T. Blackwell, Particle swarm optimization. *Swarm Intell.* **1**, 33 (2007).

13. P. Ogren, E. Fiorelli, N. E. Leonard, Cooperative control of mobile sensor networks: Adaptive gradient climbing in a distributed environment. *IEEE Trans. Automat. Contr.* **49**, 1292 (2004).

14. S. G. Reebs, Can a minority of informed leaders determine the foraging movements of a fish shoal? *Anim. Behav.* **59**, 403 (2000).

15. D. J. Hall *et al*., Diel foraging behavior and prey selection in the golden shiner (*Notemigonus crysoleucas*). *J. Fish. Board Can.* **36**, 1029 (1979).

16. Materials and methods are available as supplementary materials on *Science* Online.

17. I. D. Couzin, J. Krause, N. R. Franks, S. A. Levin, Effective leadership and decision-making in animal groups on the move. *Nature* **433**, 513 (2005).

18. M. Camperi, A. Cavagna, I. Giardina, G. Parisi, E. Silvestri, Spatially balanced topological interaction grants optimal cohesion in flocking models. *Interface Focus* **2**, 715 (2012).

19. C. J. Torney, Z. Neufeld, I. D. Couzin, Context-dependent interaction leads to emergent search behavior in social aggregates. *Proc. Natl. Acad. Sci. U.S.A.* **106**, 22055 (2009).

20. A. Huth, C. Wissel, The simulation of fish schools in comparison with experimental data. *Ecol. Modell.* **75-76**, 135 (1994).

21. U. Kils, Ph.D. thesis, University of Kiel (1987).

22. R. E. McNicol, E. Scherer, J. H. Gee, Shoaling enhances cadmium avoidance by lake whitefish, *Coregonus clupeaformis*. *Environ. Biol. Fishes* **47**, 311 (1996).

23. L. W. Hall Jr., D. T. Burton, S. L. Margrey, W. C. Graves, A comparison of the avoidance responses of individual and schooling juvenile Atlantic menhaden, *Brevoortia tyrannus* subjected to simultaneous chlorine and ΔT conditions. *J. Toxicol. Environ. Health* **10**, 1017 (1982).

24. C. W. Steele, A. D. Scarfe, D. W. Owens, Effects of group size on the responsiveness of zebrafish, *Brachydanio rerio* (Hamilton Buchanan), to alanine, a chemical attractant. *J. Fish Biol.* **38**, 553 (1991).

25. T. P. Quinn, K. Fresh, Homing and straying in chinook salmon (*Oncorhynchus tshawytscha*) from Cowlitz River Hatchery, Washington. *Can. J. Fish. Aquat. Sci.* **41**, 1078 (1984).

26. J. J. Hard, W. R. Heard, Analysis of straying variation in Alaskan hatchery chinook salmon (*Oncorhynchus tshawytscha*) following transplantation. *Can. J. Fish. Aquat. Sci.* **56**, 578 (1999).

27. K. Schaefer, D. Fuller, B. Block, Movements, behavior, and habitat utilization of yellowfin tuna (*Thunnus albacares*) in the northeastern Pacific Ocean, ascertained through archival tag data. *Mar. Biol.* **152**, 503 (2007).

28. J. García Ojalvo, J. Sancho, L. Ramírez-Piscina, A nonequilibrium phase transition with colored noise. *Phys. Rev. A* **168**, 35 (1992).

29. C. Gardiner, *Stochastic Methods: A Handbook for the Natural and Social Sciences* (Springer, New York, 2009).

30. D. Bertsekas, The auction algorithm for assignment and other network flow problems: A tutorial. *Interfaces* **20**, 133 (1990).